ACS APPLIED MATERIALS & INTERFACES

Research Article

www.acsami.org

Tailoring Dielectric and Actuated Properties of Elastomer Composites by Bioinspired Poly(dopamine) Encapsulated Graphene Oxide

Nanying Ning,[†,‡] Qin Ma,[†,‡] Suting Liu,[†,‡] Ming Tian,*[,†,‡] Liqun Zhang,[†,‡] and Toshio Nishi[§]

[†]State Key Lab of Organic−Inorganic Composites and [‡]Key Laboratory of Carbon Fiber and Functional Polymers, Ministry of Education, Beijing University of Chemical Technology, Beijing 100029, China

[§]Department of Applied Physics, The University of Tokyo, Hongo, Bunkyo-ku, Tokyo, Japan

ABSTRACT: In this study, we obtained dielectric elastomer composites with controllable dielectric and actuated properties by using a biomimetic method. We used dopamine (DA) to simultaneously coat the graphene oxide (GO) and partially reduce GO by self-polymerization of DA on GO. The poly(dopamine) (PDA) coated GO (GO-PDA) was assembled around rubber latex particles by hydrogen bonding interaction between carboxyl groups of carboxylated nitrile rubber (XNBR) and imino groups or phenolic hydroxyl groups of GO-PDA during latex compounding, forming a segregated GO-PDA network at a low percolation threshold. The results showed that the introduction of PDA on GO prevented the restack of GO in the matrix. The dielectric and actuated properties of the composites depend on the thickness of PDA shell. The dielectric loss and the elastic modulus decrease, and the breakdown strength increases with increasing the thickness of PDA shell. The maximum actuated strain increases from 1.7% for GO/XNBR composite to 4.4% for GO-PDA/XNBR composites with the PDA thickness of about 5.4 nm. The actuated strain at a low electric field (2 kV/mm) obviously increases from 0.2% for pure XNBR to 2.3% for GO-PDA/XNBR composite with the PDA thickness of 1.1 nm, much higher than that of other DEs reported in previous studies. Thus, we successfully obtained dielectric composites with low dielectric loss and improved breakdown strength and actuated strain at a low electric field, facilitating the wide application of dielectric elastomers.

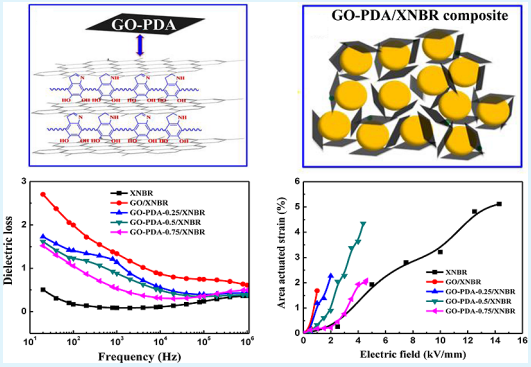

KEYWORDS: *poly(dopamine)-coated graphene oxide (GO-PDA), dielectric properties, breakdown strength, actuated strain, elastomer*

1. INTRODUCTION

Dielectric elastomers (DEs), as a kind of electroactive polymers, are capable of converting electric energy to mechanical energy and working efficiently over a broad frequency range.[1−3] DEs have good performance such as large active strain, high energy density, high electromechanical coupling efficiency, reliability, durability, fast response, and ease of processing.[4,5] Thus, DEs find applications in various devices, such as eyeball actuators,[6] tactile displays,[7] and inchworm robots,[8] and have attracted much attention in the past decades.[4,9] A disadvantage for the application of dielectric elastomer actuators (DEAs) is the requirement of high operating electric field (>100 kV/mm),[10−12] which could be harmful to humans and damage equipment, particularly in biological and medical fields.[11−13] Thus, the preparation of DEs with large actuated strain at low electric field is the biggest challenge for DEAs.

To prepare the DEs with high actuated strain at a low electric field, a high electromechanical sensitivity (β) is required, which is defined as the ratio of the dielectric constant (k) to the elastic modulus (Y) ($\beta = k/Y$). Thus, a reasonable solution to improve the β is to increase the k and decrease the Y of DEs.[14−16] One commonly used method to improve the k of an elastomer is adding high k ceramic powders such as TiO_2[17] and $BaTiO_3$[18] into the matrix. A high content (up to 50 vol %) of ceramics is usually required to obtain a high k, resulting in high elastic modulus and poor processability, thus largely limiting the applications of DEs. Another approach is to add conductive fillers such as carbon nanotubes (CNTs) and graphene sheets into the elastomer matrix.[19−23] Graphene sheets, usually synthesized from natural graphite, are more abundant, cheaper, and more easily available than CNTs. More importantly, graphene sheets with unique layered structure have a larger aspect ratio, and thus have been widely used as high k filler.[19] Usually, DEs composites with high k can be obtained by adding a small content of graphene sheets in elastomer matrix, and thus the mechanical properties can even be improved over that of pure matrix.[20,23,24] A disadvantage of the graphene sheets/elastomer composites is the increase in the dielectric loss and a sharp decrease in dielectric breakdown strength, limiting their practical applications.[25,26]

Received: January 27, 2015
Accepted: May 4, 2015
Published: May 4, 2015

DOI: 10.1021/acsami.5b00808
ACS Appl. Mater. Interfaces 2015, 7, 10755−10762

Scheme 1. Schematic Illustration of the Preparation of GO-PDA and GO-PDA/XNBR Composites

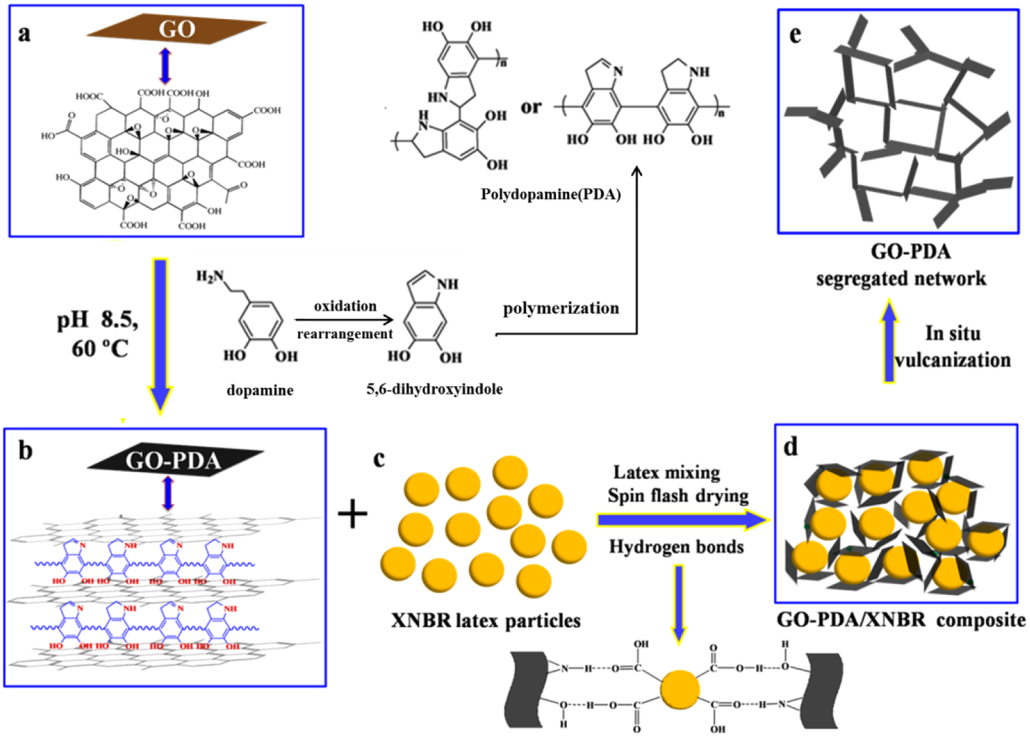

To reduce dielectric loss and increase breakdown strength of polymer/conductive filler composites, one common method is to introduce insulating modification layers on the surface of conductive fillers.[27−29] For instance, a flexible CNTs/polystyrene dielectric composites with high *k* and low dielectric loss was successfully prepared by coating an organic polypyrrole (PPy) shell on the surface of CNTs.[30] The insulating PPy shell can not only ensure the uniform dispersion of CNTs in the matrix but can also effectively stop the direct connection of CNTs from one another, and thus can decrease the dielectric loss.

Dopamine (DA) is a synthetic molecule, mimicking the mussel's foot proteins with catechol and amine functional groups. A thin poly(dopamine) (PDA) layer can be formed on the surface of a wide range of inorganic and organic materials, such as SiO_2, TiO_2, Cu, and Au, by the self-polymerization of DA in an aqueous solution.[31] Thus, the self-polymerization of DA provides an effective method for surface adhesion because of its mild reaction conditions, pollution-free features, and applicability to various materials. On the other hand, DA can act as an effective reducing agent during self-polymerization process.[30,31] Recent studies showed that DA can effectively reduce GO and give a versatile functional route.[32]

In this study, we used DA to simultaneously coat the GO and partially reduce GO by self-polymerization of DA on GO to increase the dielectric constant and breakdown strength of DEs and decrease the dielectric loss and elastic modulus of DEs. We first prepared PDA-coated GO (GO-PDA) by self-polymerization of DA on GO surface. We controlled the thickness of PDA shell by controlling the concentration of DA. The encapsulation of GO-PDA on rubber latex particles could be realized by hydrogen bonding interaction between carboxyl groups of carboxylated nitrile rubber (XNBR) and imino groups and phenolic hydroxyl groups of GO-PDA during latex compounding. Then, we studied the dependence of dielectric and actuated properties of the composites on the thickness of PDA shell. We aim to control the dielectric and actuated properties of XNBR dielectric composites by controlling the thickness of insulating PDA shell. Meanwhile, we aim to prepare dielectric elastomers with large actuated strain at a low electric field and low dielectric loss to widen the application of DEs.

2. EXPERIMENTAL SECTION

2.1. Materials. DA and tris (hydroxymethyl)-amino-methane (Tris) were purchased from Alfa Aesar Company (USA). Natural graphite (NR), XNBR, dicumyl peroxide (DCP), and potassium permanganate and all the solvent used for the preparation of graphite oxide have been described in our previous study.[23]

2.2. DA Self-Polymerization on Graphene Oxide. A uniform colloidal suspension of GO nanosheets was prepared by using the method described in our previous study.[23] The structure of GO that possesses many oxygen-containing groups is shown in Scheme 1a.

In a typical process, 100 mL of as-prepared GO colloidal suspension (1 mg/mL) and a desired amount of DA hydrochloride (50, 100, 150, 200 mg) were added into 200 mL of 10 mM Tris-Cl solution (pH 8.5) and sonicated for 10 min in an ice bath, followed by stirring vigorously at 60 °C for 24 h. Reduction of GO was simultaneously realized by oxidative polymerization of DA and PDA was adhered on double sides of GO sheet, as shown in Scheme 1b. The as-prepared PDA modified GO (GO-PDA) suspension is very stable, as evidenced by the photos of GO-PDA suspension after 24 h. After stopping the reaction, we filtered the sediment solid denoted as GO-PDA using a 0.22 μm membrane filter, and removed the residual DA by deionized water, then dried by lyophilization.[24]

2.3. Preparation of GO-PDA/XNBR Composites by Latex Mixing. The GO-PDA/XNBR composites were prepared by using the following method. 0.5 vol % of GO-PDA−X (X is the original concentration of DA (0.25, 0.5, 0.75, and 1.0 g/L)) was dispersed in aqueous solvent with ultrasonic treatment. The volume fraction of fillers used was 0.5 vol %, which was the percolation threshold of GO/XNBR composites, according to our previous study.[33] Meanwhile, 0.02 g of DCP was sonicated for 2 h to obtain a good dispersion of DCP in XNBR latex. Subsequently, the XNBR latex was mixed with the uniform GO-PDA suspension by sonication for 2 h. GO-PDA/XNBR composites

DOI: 10.1021/acsami.5b00808
ACS Appl. Mater. Interfaces 2015, 7, 10755−10762

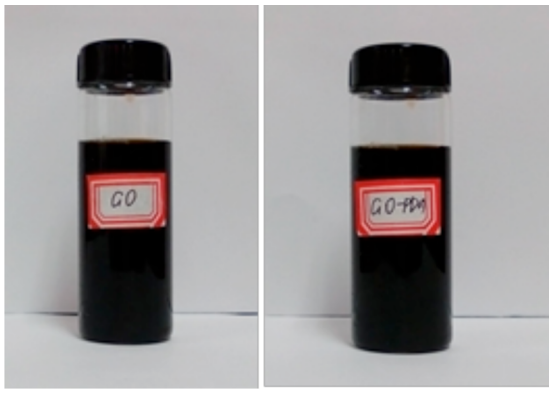

were prepared by an ultrasonically assisted latex mixing followed by a spin flash drying process. The hydrogen bonds between carboxyl groups of XNBR and imino groups and phenolic hydroxyl groups of PDA can be formed, resulting in the assembly of GO-PDA on the surface of XNBR microspheres, as shown in Scheme 1c, d. The coagulated rubber composites was then dried and vulcanized.[24] The unique GO-PDA segregated network can be formed because the cross-linked XNBR microspheres create an excluded volume and essentially push the GO-PDA distributing into the interstitial space between them, as shown in Scheme 1e. For comparison purpose, GO/XNBR composite with 0.5 vol % of GO was prepared at the same condition as that of GO-PDA/XNBR composites.

2.4. Characterization. The morphology and thickness of GO and GO-PDA-X (X = 0.25, 0.5, 0.75, and 1.0 g/L) was observed by using atomic force microscope (AFM). For each sample, the thicknesses of several pieces of GO or GO-PDA-X were tested, and the average thickness with experiment error was reported. X-ray photoelectron spectroscopy (XPS) was used to study the chemical compositions of graphite oxide, DA, and GO-PDA. UV−vis absorption spectrum and thermal gravity analysis (TGA) were used to assess the reduction degree of GO induced by DA with different concentration.

The morphology of GO/XNBR and GO-PDA/XNBR composites was obtained by high resolution transmission electron microscopy. The Volume resistivity (ρv), the dielectric properties, the elastic modulus (Y) and the actuated strain of pure XNBR, GO/XNBR and GO-PDA/XNBR composites were obtained following the methods described in our previous study.

All the equipment, the sample preparation methods and the corresponding test conditions for each characterization were the same as that used in our previous study.[23,24,33] Every experimental data in this study is the average of the results obtained from at least three samples under the same conditions.

3. RESULTS AND DISCUSSION

3.1. Self-Polymerization of DA on GO. The encapsulation of PDA on GO was determined by XPS and AFM. Figure 1a shows the wide-scan XPS spectra of GO and GO-PDA. Compared with the spectra of GO, the spectra of GO-PDA exhibits a new peak at about 400 eV, representing the N 1s electron of the DA on GO-PDA. The fitted curve of the N 1s spectrum of GO-PDA is shown in the inset of Figure 1a. We observe two peaks: one peak at 399.5 eV corresponding to the amine (−N−H) groups from DA and the other peak at 398.5 eV corresponding to the imine (═N−) groups formed by the indole groups through structure evolution during the self-polymerization of DA.[34] Figure 1b shows the high-resolution XPS spectra of GO and GO-PDA. We can observe four characteristic peaks corresponding to carbon atoms in different functional groups of both GO and GO-PDA: C−C at 284.6 eV, C−O at 286.4 eV, C═O at 287.8 eV, and COOH at 288.9 eV.[23] We also observe a new peak at 285.5 eV on the spectrum of GO-PDA, representing the C−N peak from DA, suggesting that PDA have been successfully adhered on GO through the self-polymerization of DA.

The morphology and thickness of GO and GO-PDA nanosheets was examined by using AFM to further verify the

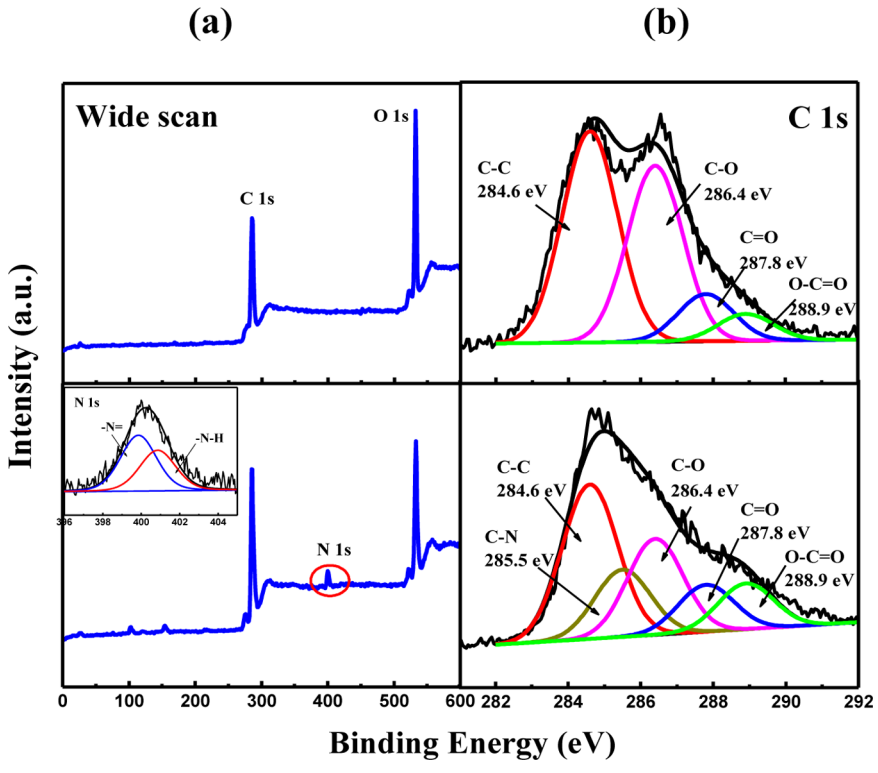

Figure 1. (a) XPS wide scan and (b) C 1s core-level spectra of GO and GO-PDA, and (inset) the N 1s core-level spectrum of GO-PDA.

DOI: 10.1021/acsami.5b00808
ACS Appl. Mater. Interfaces 2015, 7, 10755−10762

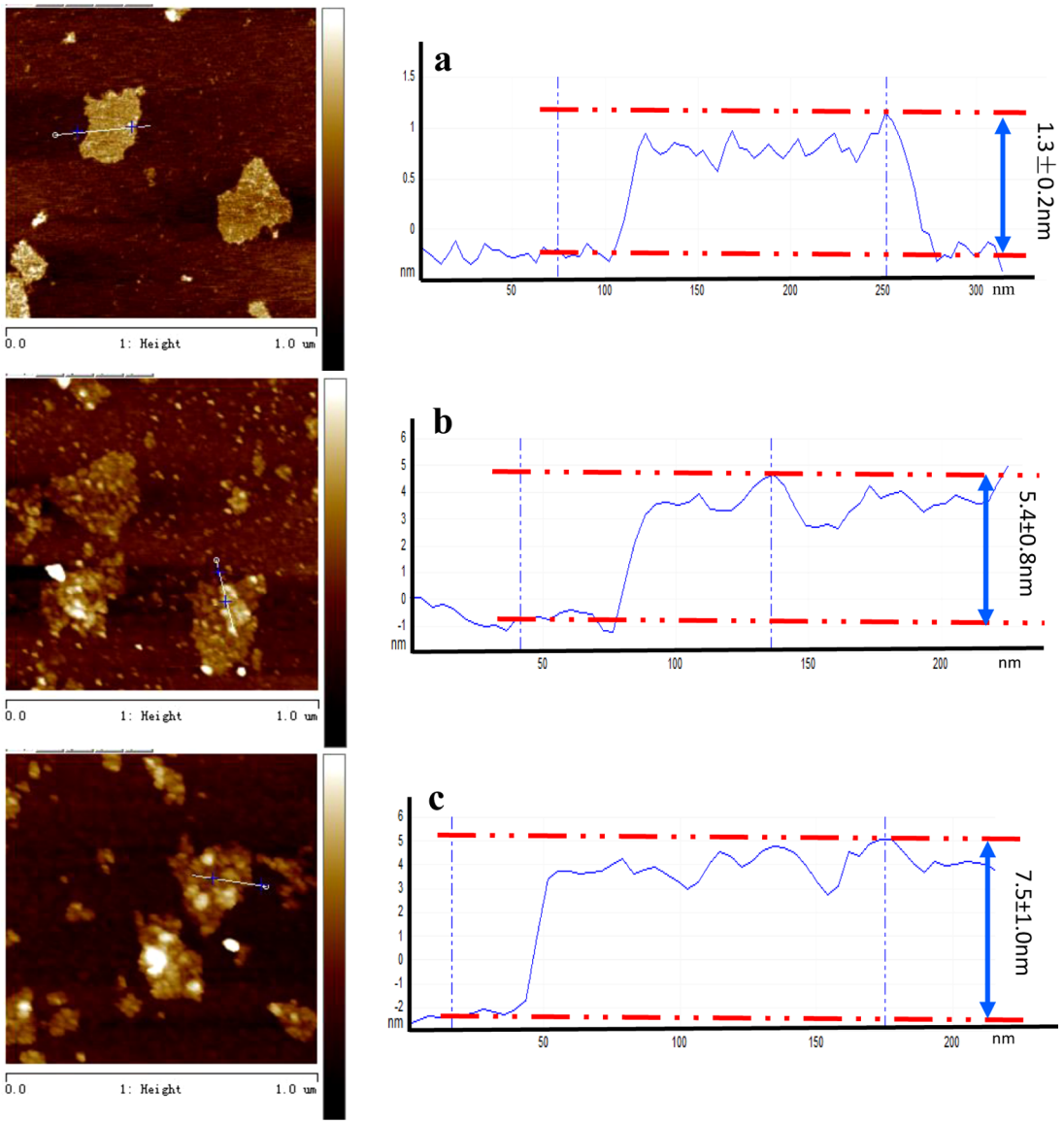

Figure 2. AFM height images of (a) GO, (b) GO-PDA-0.5, and (c) GO-PDA-1.0 nanosheets; (a′−c′) cross-section analyses along the lines shown in AFM images show the heights of GO, GO-PDA-0.5, and GO-PDA-1.0 nanosheets, respectively.

adhesion of PDA on GO. Figure 2 shows the AFM height images of GO, GO-PDA−0.5 and GO-PDA-1.0. The average thickness of GO (∼1.3 nm) is slightly larger than that of single sheet of graphene because of the presence of oxygen-containing groups, as shown in Figure 2a.[34,35] The thickness of PDA-functionalized GO at the DA concentration of 0.5 and 1.0 g/L (GO-PDA-0.5) increases to 5.4 ± 0.5 nm and 7.5 ± 0.5 nm, respectively (see Figure 2b, c), indicating that PDA has been successfully adhered on GO through the self-polymerization of DA on GO. Obviously, we can tune the thickness of GO-PDA by tuning the concentration of DA. In addition, we can see that dopamine can self-polymerize in solution to form PDA nanoparticles closely coated on the surface of GO, as has been reported in previous studies.[35,36] The error of the thickness of these GO-PDA nanosheets treated at certain DA concentration is ±0.5 nm.

The dependence of PDA shell thickness of GO-PDA on the concentration of DA is shown in Figure 3. Here, we should note that the PDA shell thickness of GO-PDA is half of the difference between the thickness of GO and GO-PDA because PDA was adhered on double sides of GO. Interestingly, the PDA shell

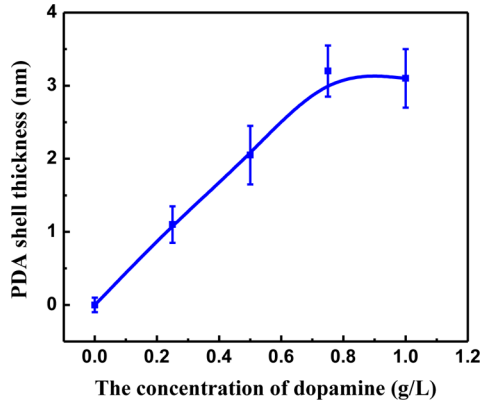

Figure 3. Dependence of PDA shell thickness on the concentration of dopamine.

thickness is almost proportional to the concentration of DA when the concentration of DA is below 0.75 g/L. Therefore, we can control the PDA shell thickness by tuning the concentration

DOI: 10.1021/acsami.5b00808
ACS Appl. Mater. Interfaces 2015, 7, 10755−10762

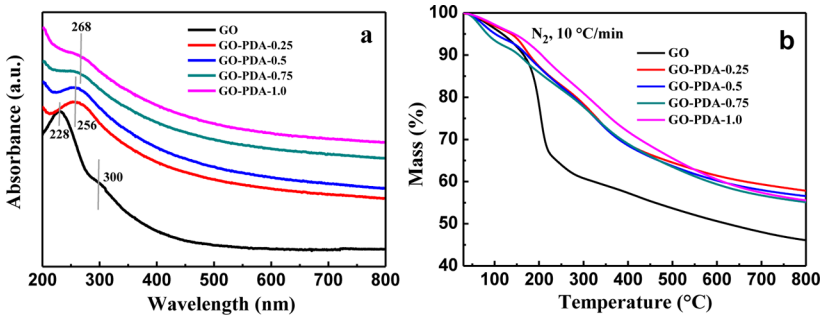

Figure 4. (a) UV−vis absorption spectra and (b) TGA curves of GO and GO-PDA-X (X = 0.25, 0.5, 0.75, 1.0).

of DA. The increase in PDA shell thickness slows down when the concentration of DA exceeds 0.75 g/L because DA at high concentration tends to self-polymerize in aqueous instead of depositing on the surface of GO.

3.2. DA-Induced Reduction of GO. The degree of reduction of GO by different concentrations of DA was examined by using UV−vis spectra and TGA. The UV−vis spectra of GO and GO-PDA are shown in Figure 4a. GO shows two characteristic peaks at 228 and 300 nm, respectively. The peak at 228 nm of GO shifts to 256 nm for GO-PDA-0.25 and GO-PDA-0.5, it further shifts to 268 nm for GO-PDA-0.75 and GO-PDA-1.0, indicating that GO is partially reduced by DA and the degree of reduction of GO increases with increasing concentration of DA.[37,38]

Figure 4b shows the TGA curves of GO and GO-PDA at a heating rate of 10 °C min^{-1} in nitrogen atmosphere. The maximum rate of mass loss occurs at 170−230 °C for GO, corresponding to the loss of most of the oxygen-containing groups. Compared with GO, the mass loss of GO-PDA at the same temperature (180−800 °C) largely decreases, again suggesting the partial reduction of GO by DA. The total mass loss of GO-PDA nanosheets slightly increased with the increase in the concentration of DA, indicating the increase in the content of PDA. With the increase in the concentration of DA, the trend of thermal weight loss of GO-PDA grows closer to that of RGO,[23] indicating the higher reduction degree of GO.

3.3. Microstructure of GO-PDA/XNBR Composites. The TEM pictures of GO/XNBR and GO-PDA/XNBR composites are shown in Figure 5. The darker lines are GO, GO-PDA-0.5 or GO-PDA-1.0, and the gray part are XNBR latex particles. The segregated network structure with a large number of GO uniformly distributed around the surface of XNBR latex particles and connected with one another is formed in GO/XNBR composite (see Figure 5a), as reported in the previous study.[24] Interestingly, similar segregated network structure with GO-PDA evenly distributed around the XNBR latex particles and connected with one another are observed in both composites with GO-PDA-0.5 and GO-PDA-1.0 (see Figure 5c, e). The assembly between GO-PDA and XNBR latex particles is caused by the hydrogen-bonding interactions between imino groups or phenolic hydroxyl groups of PDA and carboxyl groups of XNBR latex at the interface.

To determine the thickness of GO, GO-PDA-0.5, and GO-PDA-1 in the composites, TEM images with higher resolution were obtained, as shown in Figure 5b, d, and f, respectively. The thickness of GO in the composite is about 10 nm (see Figure 5b), indicating the restacking of 8 layers of single layer GO in the polymer matrix caused by the $\pi-\pi$ stacking and hydrophobic interactions of GO during sample preparation process. The

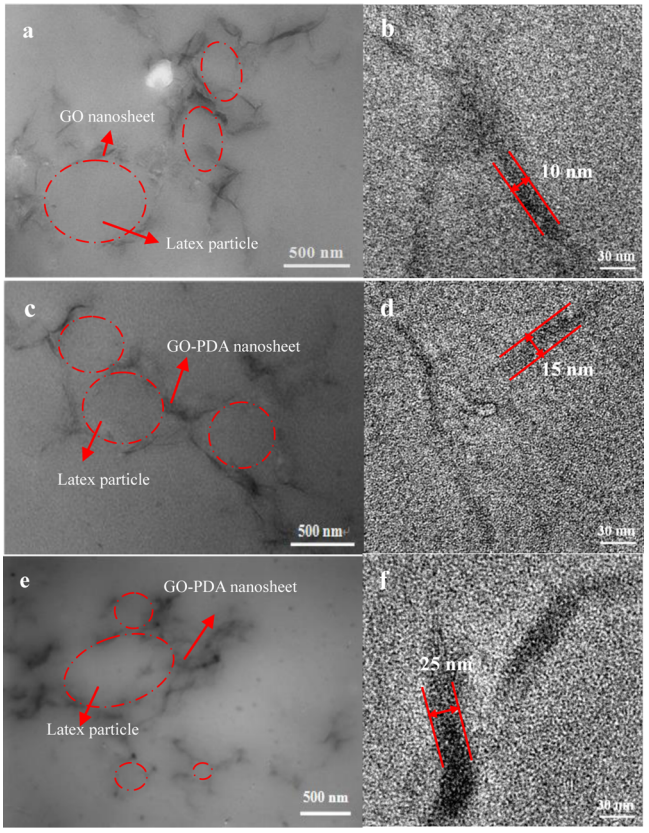

Figure 5. HRTEM images of (a, b) GO/XNBR, (c, d) GO-PDA-0.5/XNBR, and (e, f) GO-PDA-1.0/XNBR composites.

thickness of GO-PDA-0.5 and GO-PDA-1.0 in the composites increases to 15 and 25 nm (see Figure 5d, f). According to the thickness of as-prepared GO-PDA-0.5 nanosheets (5.4 nm) and GO-PDA-1.0 nanosheets (8.5 nm) (see Figure 2), we can conclude that 3 layers of single layer GO-PDA are stacked in both composites with GO-PDA-0.5 and GO-PDA-1.0. Therefore, the introduction of PDA on the surface of GO nanosheets can effectively prevent the severe stacking of GO in the rubber matrix, suggesting a dielectric filler network could be formed by using less content of GO.

3.4. Electromechanical Properties of GO-PDA/XNBR Composites. Figure 6 presents the dielectric properties versus frequency of pure XNBR, GO/XNBR, and GO-PDA/XNBR composites at room temperature. We can observe that the k of all the composites decreases with increasing the frequency (see Figure 6a), indicating that the frequency dependence of k is strong for all the composites, ascribed to the accumulation of many free charges at the internal interfaces between GO or GO-

DOI: 10.1021/acsami.5b00808
ACS Appl. Mater. Interfaces 2015, 7, 10755−10762

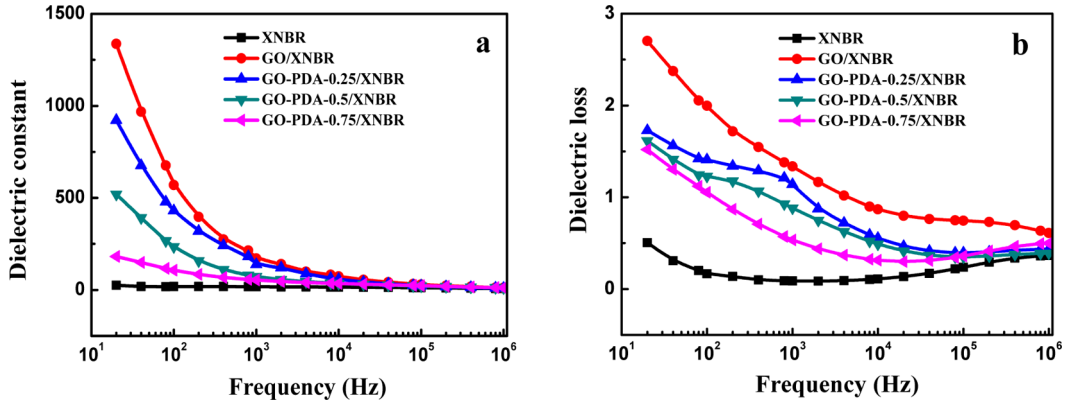

Figure 6. Frequency dependence of (a) dielectric constant and (b) dielectric loss of GO-PDA/XNBR composites with different concentration of dopamine.

PDA and XNBR (named as interfacial polarization effect).[39,40] Compared with pure XNBR, the *k* of GO/XNBR composite with 0.5 vol % GO is sharply increased, demonstrating that GO can effectively improve the *k* of XNBR, as reported in our previous studies.[24] The *k* at the same frequency decreases with the increase in the thickness of PDA shell on GO.

The frequency dependence of the dielectric loss of the composites with the thickness of PDA shell is shown in Figure 6b. Likewise, an obvious frequency dependence of dielectric loss is observed for all the composites. Compared with pure XNBR, the dielectric loss of GO/XNBR composite with 0.5 vol % GO obviously increases, especially at the low frequency, ascribed to the relatively high DC conductance (see below). Importantly, the dielectric loss of GO-PDA/XNBR composites decreases with increasing the thickness of PDA shell.

To study the effect of the thickness of PDA shell on the dielectric properties of the composites, the *k* and dielectric loss at 1×10^3 Hz and the conductivity of the composites are presented in Figure 7. The electrical conductivity of the composites

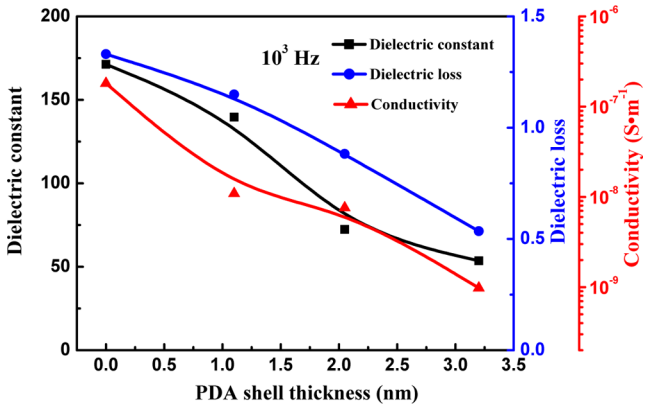

Figure 7. Dependence of the dielectric constant at 1×10^3 Hz, dielectric loss at 1×10^3 Hz and conductivity of GO-PDA/XNBR composites on the thickness of PDA shell.

decreases with the increase in the thickness of PDA shell. For example, the electrical conductivity obviously decreases from 1.8×10^{-7} S/m for GO/XNBR composite to 1.1×10^{-8} S/m for GO-PDA−0.25/XNBR composite with the PDA shell thickness of 1.1 nm and it further decreases to 9.8×10^{-10} S/m for GO-PDA−0.75/XNBR composite with the PDA shell thickness of 3.2 nm. Therefore, the introduction of PDA shell changes the GO/XNBR composite from semiconductor to insulator. Here, two effects affect the conductivity of the composites. One effect is the increase in reduction degree of GO by PDA, resulting in the increase in conductivity of GO-PDA. The other effect is the insulativity of PDA shell on GO, leading to the decrease in conductivity of GO-PDA. Obviously, despite of the increase in the reduction degree of GO with the increase in the thickness of PDA shell, the insulating PDA shell on GO plays a dominate role, resulting in the decrease in conductivity. As a result, both *k* and dielectric loss decrease obviously with the increase in the thickness of PDA shell. The *k* at 1×10^3 Hz decreases from 171 for GO/XNBR composite to 139 for GO-PDA-0.25/XNBR composite and 72 for GO-PDA-0.5/XNBR composite, and the dielectric loss at 1×10^3 Hz decreases from 1.33 for GO/XNBR composite to 1.14 for GO-PDA-0.25/XNBR composite and 0.88 for GO-PDA-0.5/XNBR composite. The decrease in *k* of the composites with the increase in PDA shell thickness is ascribed to the decrease in the interfacial polarization of GO-PDA composites caused by the insulativity of PDA shell. The decrease in dielectric loss of the composites with increasing the PDA shell thickness is caused by the decrease in DC conductance of GO-PDA composites by the insulating PDA shell. Therefore, we can control the dielectric properties of GO-PDA/XNBR composites by tuning the thickness of PDA shell via controlling the concentration of DA.

The *Y* and β of pure XNBR, GO/XNBR, and GO-PDA/XNBR composites are shown in Table 1. The *Y* of the composite decreases with increasing the thickness of PDA shell. Despite of the decrease in *Y*, the β at 1×10^3 Hz decreases with increasing the thickness of PDA shell because of the decrease in *k*.

Figure 8 presents the actuated strains versus electric fields of pure XNBR and the composites. The actuated strain of all the samples obviously increases with increasing the electric field, as reported in previous studies.[24] The breakdown strength sharply decreases from 14 kV/mm for pure XNBR to 1 kV/mm for GO/XNBR composite with 0.5 vol % GO because of the large increase in DC conductivity and dielectric loss with the addition of 0.5 vol % GO. Meanwhile, the maximum actuated strain largely decreases from 5.1% for pure XNBR to 1.7% for GO/XNBR composite with 0.5 vol % GO. Interestingly, the breakdown strength of the composites obviously increases with increasing thickness of the PDA shell, ascribed to the decrease in DC conductivity and dielectric loss with the increase in PDA shell thickness. The maximum actuated strain increases from 1.7% for GO/XNBR composite to 4.4% for GO-PDA-0.5/XNBR composites with the PDA thickness of 5.4 nm. Although the

DOI: 10.1021/acsami.5b00808
ACS Appl. Mater. Interfaces 2015, 7, 10755−10762

Table 1. Elastic Modulus, Dielectric Properties, and Actuated Strain of Pure XNBR and XNBR with 0.5 vol % GO and GO-PDA-X (X = 0.25, 0.5, 0.75, and 1.0)

filler (0.5 vol %)	elastic modulus Y (MPa)	$\beta = k/Y$ (MPa^{-1})	breakdown strength (kV/mm)	maximal actuated strain (%)	actuated strain at 2 kV/mm (%)	actuated strain at 4 kV/mm (%)
pure XNBR	1.7 ± 0.1	14.7	14.3	5.1@14.3 kV/mm	0.2 ± 0.01	1.2 ± 0.1
GO	3.9 ± 0.3	43.8	1.0	1.7@1 kV/mm		
GO-PDA-0.25	3.6 ± 0.2	38.6	2.0	2.3@2 kV/mm	2.3 ± 0.2	
GO-PDA-0.5	3.1 ± 0.2	23.2	4.4	4.4@4.4 kV/mm	0.9 ± 0.03	3.8 ± 0.2
GO-PDA-0.75	2.7 ± 0.1	20.0	4.6	2.1@4.6 kV/mm	0.3 ± 0.02	1.9 ± 0.15

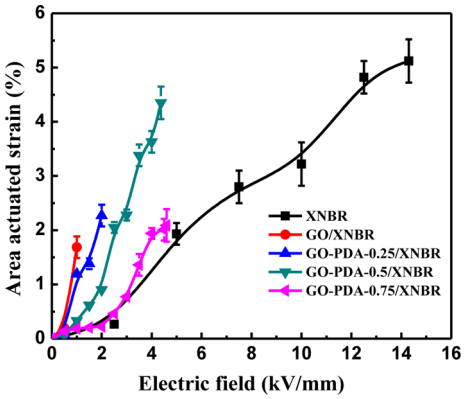

Figure 8. Actuated strain of GO/XNBR and GO-PDA-X (X = 0.25, 0.5, 0.75, 1.0)/XNBR composites.

maximum actuated strain of GO-PDA-0.5/XNBR composite is slightly lower than that of pure XNBR, the applied electric field of the composite is much lower. Importantly, the actuated strain at low electric fields of GO-PDA/XNBR composites is much higher than that of pure XNBR, as shown in Table 1. For instance, the actuated strain at 4 kV/mm increases from 1.20% for pure XNBR to 3.8% for GO-PDA-0.5/XNBR composite. Moreover, the actuated strain at 2 kV/mm of pure XNBR increases from 0.23 to 2.3% with the addition of 0.5 vol % of GO-PDA-0.25, much higher than that of other previously reported DEs,[11,34,41−47] as summarized in Table 2. The improvement in actuated strain at low electric fields is in favor of the application of DE in biological and medical fields (such as artificial skin), tactile displays, and braille displays, etc.[48]

Table 2. Comparison of Actuated Performances of Advanced DE Composites

composites	maximum actuated strain (%)	actuated strain at 2 kV/mm (%)
PHT/PDMS[11]	8.0 (8 kV/mm)	0.4
PDVB@PANI/PDMS[40]	16.0 (43 kV/mm)	0.01
PMN/PDMS[41]	8.0 (53 kV/mm)	<1.0
dipoles-PDMS[42]	1.4 (16 kV/mm)	<0.01
TiO_2−PDMS (plasticized)[43]	18.0 (37 kV/mm)	<1.0
allyl-cyano filled silicon[44]	10.0 (48 kV/mm)	<0.01
$BaTiO_3$−PDA/HNBR[33]	20.0 (45 kV/mm)	<2.0
PANI-polyCuPc/PU[45]	7.0 (23 kV/mm)	<0.1
polyester elastomer[46]	12.0 (15 kV/mm)	<1.0
GO-PDA-0.25/XNBR in our study	2.27 (2.0 kV/mm)	2.27

CONCLUSIONS

We fabricated dielectric elastomer composites with controllable dielectric and actuated properties by using a biomimetic method. The self-polymerization of DA on GO simultaneously realized the coat of PDA on GO and the partial reduction of GO. A segregated GO-PDA network at a low percolation threshold was formed by self-assembling of GO-PDA around XNBR latex particles during latex compounding because of the hydrogen bonding interaction between XNBR and GO-PDA. The restack of GO in the matrix was effectively prevented by the coat of PDA on GO. The dielectric and actuated properties of the composites can be controlled by the thickness of PDA shell. The dielectric composites with low dielectric loss and improved breakdown strength and actuated strain at a low electric field were successfully obtained for the wide application of dielectric elastomers.

AUTHOR INFORMATION

Corresponding Author

*E-mail: tianm@mail.buct.edu.cn. Tel.: +86 10 6443 4860. Fax: +86 10 6443 3964.

Notes

The authors declare no competing financial interest.

ACKNOWLEDGMENTS

The financial support of the National Natural Science Foundation of China (Grants 51173007 and 51221002) is gratefully acknowledged.

REFERENCES

(1) Rao, Y.; Wong, C. P. Material characterization of a high-dielectric-constant polymer-ceramic composite for embedded capacitor for RF applications. *J. Appl. Polym. Sci.* **2004**, *92*, 2228−2231.

(2) Song, Y.; Shen, Y.; Liu, H.; Lin, Y.; Li, M.; Nan, C. Improving the Dielectric Constants and Breakdown Strength of Polymer Composites: Effects of BaTiO3 Nanoinclusions Shape, Surface Modification and Polymer Matrice. *J. Mater. Chem.* **2012**, *22*, 16491−16498.

(3) Stoyanov, H.; Kollosche, M.; Risse, S.; McCarthy, D. N.; Kofod, G. Elastic block copolymer nanocomposites with controlled interfacial interactions for artificial muscles with direct voltage control. *Soft Matter* **2011**, *7*, 194−202.

(4) Shankar, R.; Ghosh, T. K.; Spontak, R. J. Dielectric elastomers as next-generation polymeric actuators. *Soft Matter* **2007**, *3*, 1116−1129.

(5) Pelrine, R.; Kornbluh, R.; Joseph, J.; Heydt, R.; Pei, Q.; Chiba, S. High-field deformation of elastomeric dielectrics for actuators. *Mater. Sci. Eng., C* **2000**, *11*, 89−100.

(6) Suo, Z. Theory of dielectric elastomers. *Acta Mech. Solida Sin.* **2010**, *23*, 549−578.

(7) Todd, M. G.; Shi, F. G. Characterizing the interphase dielectric constant of polymer composite materials: Effect of chemical coupling agents. *J. Appl. Phys.* **2003**, *94*, 4551−4557.

DOI: 10.1021/acsami.5b00808
ACS Appl. Mater. Interfaces 2015, 7, 10755−10762

(8) Li, Z.; Fredin, L. A.; Tewari, P.; DiBenedetto, S. A.; Lanagan, M. T.; Ratner, M. A.; Marks, T. J. In Situ Catalytic Encapsulation of Core-Shell Nanoparticles Having Variable Shell Thickness: Dielectric and Energy Storage Properties of High-Permittivity Metal Oxide Nanocomposites. *Chem. Mater.* **2010**, *22*, 5154−5164.
(9) Potts, J. R.; Dreyer, D. R.; Bielawski, C. W.; Ruoff, R. S. Graphene-based polymer nanocomposites. *Polymer* **2011**, *52*, 5−25.
(10) Chen, L. Z.; Liu, C. H.; Hu, C. H.; Fan, S. S. Electrothermal actuation based on carbon nanotube network in silicone elastomer. *Appl. Phys. Lett.* **2008**, *92*, 263104−1−3.
(11) Carpi, F.; Gallone, G.; Galantini, F.; De Rossi, D. Silicone−Poly(hexylthiophene) Blends as Elastomers with Enhanced Electromechanical Transduction Properties. *Adv. Funct. Mater.* **2008**, *18*, 235−241.
(12) Huang, C.; Zhang, Q. Enhanced Dielectric and Electromechanical Responses in High Dielectric Constant All-Polymer Percolative Composites. *Adv. Funct. Mater.* **2004**, *14*, 501−506.
(13) Molberg, M.; Leterrier, Y.; Plummer, C. J. G.; Walder, C.; Löwe, C.; Opris, D. M.; Nüesch, F. A.; Bauer, S.; Månson, J.-A. E. Frequency dependent dielectric and mechanical behavior of elastomers for actuator applications. *J. Appl. Phys.* **2009**, *106*, 054112.
(14) OHalloran, A.; OMalley, F.; McHugh, P. A review on dielectric elastomer actuators, technology, applications, and challenges. *J. Appl. Phys.* **2008**, *104*, 071101−071101−10.
(15) Wissler, M.; Mazza, E. Electromechanical coupling in dielectric elastomer actuators. *Sensor. Actuat. A-Phys.* **2007**, *138*, 384−393.
(16) Kofod, G.; Somrner-Larsen. Some Aspects of Large Strain Actuation in Dielectric Elastomers. Electrets, 2005. ISE-12. *2005 12th International Symposium on* **2005**, 208−211.
(17) Carpi, F.; Rossi, D. D. Improvement of electromechanical actuating performances of a silicone dielectric elastomer by dispersion of titanium dioxide powder. *IEEE T. Dielect. El. In.* **2005**, *12*, 835−843.
(18) Cherney, E. Silicone rubber dielectrics modified by inorganic fillers for outdoor high voltage insulation applications. *IEEE T. Dielect. El. In.* **2005**, *12*, 1108−1115.
(19) Romasanta, L. J.; Hernández, M.; López-Manchado, M. A.; Verdejo, R. Functionalised graphene sheets as effective high dielectric constant fillers. *Nanoscale Res. Lett.* **2011**, *6*, 1−6.
(20) Wu, C.; Huang, X.; Wang, G.; Wu, X.; Yang, K.; Li, S.; Jiang, P. Hyperbranched-polymer functionalization of graphene sheets for enhanced mechanical and dielectric properties of polyurethane composites. *J. Mater. Chem.* **2012**, *22*, 7010−7019.
(21) Seveyrat, L.; Chalkha, A.; Guyomar, D.; Lebrun, L. Preparation of graphene nanoflakes/polymer composites and their performances for actuation and energy harvesting applications. *J. Appl. Phys.* **2012**, *111*, 104904−104904−9.
(22) Wang, Z.; Nelson, J. K.; Hillborg, H.; Zhao, S.; Schadler, L. S. Graphene oxide filled nanocomposite with novel electrical and dielectric properties. *Adv. Mater.* **2012**, *24*, 3134−3137.
(23) Liu, S.; Tian, M.; Yan, B.; Yao, Y.; Zhang, L.; Nishi, T.; Ning, N. High performance dielectric elastomers by partially reduced graphene oxide and disruption of hydrogen bonding of polyurethanes. *Polymer* **2014**, *56*, 375−384.
(24) Tian, M.; Ma, Q.; Li, X.; Zhang, L.; Nishi, T.; Ning, N. High performance dielectric composites by latex compounding of graphene oxide-encapsulated carbon nanosphere hybrids with XNBR. *J. Mater. Chem. A* **2014**, *2*, 11144−11154.
(25) Lu, J.; Moon, K.-S.; Xu, J.; Wong, C. Synthesis and dielectric properties of novel high-K polymer composites containing in-situ formed silver nanoparticles for embedded capacitor applications. *J. Mater. Chem.* **2006**, *16*, 1543−1548.
(26) Yuan, J.-K.; Dang, Z.-M.; Yao, S.-H.; Zha, J.-W.; Zhou, T.; Li, S.-T.; Bai, J. Fabrication and dielectric properties of advanced high permittivity polyaniline/poly (vinylidene fluoride) nanohybrid films with high energy storage density. *J. Mater. Chem.* **2010**, *20*, 2441−2447.
(27) Shen, Y.; Lin, Y.; Nan, C. W. Interfacial Effect on Dielectric Properties of Polymer Nanocomposites Filled with Core/Shell-Structured Particles. *Adv. Funct. Mater.* **2007**, *17*, 2405−2410.
(28) Shen, Y.; Lin, Y.; Li, M.; Nan, C. W. High dielectric performance of polymer composite films induced by a percolating interparticle barrier layer. *Adv. Mater.* **2007**, *19*, 1418−1422.
(29) Kuang, X.; Liu, Z.; Zhu, H. Dielectric properties of Ag@ C/PVDF composites. *J. Appl. Polym. Sci.* **2013**, *129*, 3411−3416.
(30) Yang, C.; Lin, Y.; Nan, C. Modified carbon nanotube composites with high dielectric constant, low dielectric loss and large energy density. *Carbon* **2009**, *47*, 1096−1101.
(31) Lee, H.; Dellatore, S. M.; Miller, W. M.; Messersmith, P. B. Mussel-inspired surface chemistry for multifunctional coatings. *Science* **2007**, *318*, 426−430.
(32) Kang, S. M.; Park, S.; Kim, D.; Park, S. Y.; Ruoff, R. S.; Lee, H. Simultaneous Reduction and Surface Functionalization of Graphene Oxide by Mussel - Inspired Chemistry. *Science* **2007**, *318*, 426−430.
(33) Tian, M.; Zhang, J.; Zhang, L.; Liu, S.; Zan, X.; Nishi, T.; Ning, N. Graphene encapsulated rubber latex composites with high dielectric constant, low dielectric loss and low percolation threshold. *J. Colloid Interface Sci.* **2014**, *430*, 249−256.
(34) Yang, D.; Tian, M.; Li, D.; Wang, W.; Ge, F.; Zhang, L. Enhanced dielectric properties and actuated strain of elastomer composites with dopamine-induced surface functionalization. *J. Mater. Chem. A* **2013**, *1*, 12276−12284.
(35) Jiang, J.; Zhu, L.; Zhu, L.; Zhu, B.; Xu, Y. Surface characteristics of a self-polymerized dopamine coating deposited on hydrophobic polymer films. *Langmuir* **2011**, *27*, 14180−14187.
(36) Zhang, W.; Yang, F. K.; Han, Y.; Gaikwad, R.; Leonenko, Z.; Zhao, B. Surface and tribological behaviors of the bioinspired polydopamine thin films under dry and wet conditions. *Biomacromolecules* **2013**, *14*, 394−405.
(37) Novoselov, K. S.; Geim, A. K.; Morozov, S.; Jiang, D.; Zhang, Y.; Dubonos, S.; Grigorieva, I.; Firsov, A. Electric field effect in atomically thin carbon films. *Science* **2004**, *306*, 666−669.
(38) Novoselov, K.; Jiang, D.; Schedin, F.; Booth, T.; Khotkevich, V.; Morozov, S.; Geim, A. Two-dimensional atomic crystals. *P. Natl. Acad. Sci. U.S.A.* **2005**, *102*, 10451−10453.
(39) Huang, X.; Jiang, P.; Xie, L. Ferroelectric polymer/silver nanocomposites with high dielectric constant and high thermal conductivity. *Appl. Phys. Lett.* **2009**, *95*, 242901−242901−3.
(40) Dang, Z. M.; Wang, L.; Yin, Y.; Zhang, Q. Giant Dielectric Permittivities in Functionalized Carbon - Nanotube/Electroactive-Polymer Nanocomposites. *Adv. Mater.* **2007**, *19*, 852−857.
(41) Opris, D. M.; Molberg, M.; Walder, C.; Ko, Y. S.; Fischer, B.; Nüesch, F. A. New silicone composites for dielectric elastomer actuator applications in competition with acrylic foil. *Adv. Funct. Mater.* **2011**, *21*, 3531−3539.
(42) Yang, D.; Zhang, L.; Liu, H.; Dong, Y.; Yu, Y.; Tian, M. Lead magnesium niobate-filled silicone dielectric elastomer with large actuated strain. *J. Appl. Polym. Sci.* **2012**, *125*, 2196−2201.
(43) Kussmaul, B.; Risse, S.; Kofod, G.; Waché, R.; Wegener, M.; McCarthy, D. N.; Krüger, H.; Gerhard, R. Enhancement of dielectric permittivity and electromechanical response in silicone elastomers: Molecular grafting of organic dipoles to the macromolecular network. *Adv. Funct. Mater.* **2011**, *21*, 4589−4594.
(44) Zhao, H.; Wang, D.-R.; Zha, J.-W.; Zhao, J.; Dang, Z.-M. Increased electroaction through a molecular flexibility tuning process in TiO2−polydimethylsilicone nanocomposites. *J. Mater. Chem. A* **2013**, *1*, 3140−3145.
(45) Risse, S.; Kussmaul, B.; Krüger, H.; Kofod, G. Synergistic improvement of actuation properties with compatibilized high permittivity filler. *Adv. Funct. Mater.* **2012**, *22*, 3958−3962.
(46) Huang, C.; Zhang, Q. M. Fully Functionalized High-Dielectric-Constant Nanophase Polymers with High Electromechanical Response. *Adv. Mater.* **2005**, *17*, 1153−1158.
(47) Yang, D.; Tian, M.; Kang, H.; Dong, Y.; Liu, H.; Yu, Y.; Zhang, L. New polyester dielectric elastomer with large actuated strain at low electric field. *Mater. Lett.* **2012**, *76*, 229−232.
(48) Carpi, F.; Bauer, S.; De Rossi, D. Materials Science. Stretching Dielectric Elastomer Performance. *Science* **2010**, *330*, 1759−1761.

DOI: 10.1021/acsami.5b00808
ACS Appl. Mater. Interfaces 2015, 7, 10755−10762